THE JOURNAL OF BIOLOGICAL CHEMISTRY VOL. 289, NO. 15, pp. 10419–10430, April 11, 2014

The Mechanism of Membrane Disruption by Cytotoxic Amyloid Oligomers Formed by Prion Protein(106–126) Is Dependent on Bilayer Composition*[S]

Received for publication, September 4, 2013, and in revised form, February 1, 2014 Published, JBC Papers in Press, February 19, 2014, DOI 10.1074/jbc.M113.515866

Patrick Walsh[‡§1], **Gillian Vanderlee**[¶], **Jason Yau**[‡§2], **Jody Campeau**[‖], **Valerie L. Sim**[‖3], **Christopher M. Yip**[§¶], **and Simon Sharpe**[‡§4]

From the [‡]*Molecular Structure and Function Program, The Hospital for Sick Children, Toronto, Ontario M5G 1X8, the* [§]*Department of Biochemistry, University of Toronto, Toronto, Ontario M5S 1A8, the* [¶]*Institute of Biomaterials and Biomedical Engineering, Terrence Donnelly Centre for Cellular and Biomolecular Research, University of Toronto, Toronto, Ontario M5S 3E1, and the* [‖]*Department of Medicine, Division of Neurology, University of Alberta, Edmonton, Alberta T6G 2G3, Canada*

Background: Nonfibrillar amyloid oligomers are cytotoxic and may act through physical disruption of cell membranes.
Results: Cytotoxic oligomers of the amyloid peptide PrP(106–126) disrupt membranes through distinct mechanisms, depending on lipid composition.
Conclusion: Cytotoxicity of PrP(106–126) oligomers can occur through at least two different physical processes.
Significance: Mechanisms for the membrane disruption of amyloid oligomers are proposed, providing new insight into their cytotoxicity.

The formation of fibrillar aggregates has long been associated with neurodegenerative disorders such as Alzheimer and Parkinson diseases. Although fibrils are still considered important to the pathology of these disorders, it is now widely understood that smaller amyloid oligomers are the toxic entities along the misfolding pathway. One characteristic shared by the majority of amyloid oligomers is the ability to disrupt membranes, a commonality proposed to be responsible for their toxicity, although the mechanisms linking this to cell death are poorly understood. Here, we describe the physical basis for the cytotoxicity of oligomers formed by the prion protein (PrP)-derived amyloid peptide PrP(106–126). We show that oligomers of this peptide kill several mammalian cells lines, as well as mouse cerebellar organotypic cultures, and we also show that they exhibit antimicrobial activity. Physical perturbation of model membranes mimicking bacterial or mammalian cells was investigated using atomic force microscopy, polarized total internal reflection fluorescence microscopy, and NMR spectroscopy. Disruption of anionic membranes proceeds through a carpet or detergent model as proposed for other antimicrobial peptides. By contrast, when added to zwitterionic membranes containing cholesterol-rich ordered domains, PrP(106–126) oligomers induce a loss of domain separation and decreased membrane disorder. Loss of raft-like domains may lead to activation of apoptotic pathways, resulting in cell death. This work sheds new light on the physical mechanisms of amyloid cytotoxicity and is the first to clearly show membrane type-specific modes of action for a cytotoxic peptide.

The study of amyloids and their related toxicity is an important aspect of understanding the onset and progression of several neurodegenerative diseases, including Alzheimer, Parkinson, and prion diseases, among others (1–3). In each case, misfolding and aggregation of a native protein leads to cell death through mechanisms that are not yet understood. Although the characteristic pathology of amyloid disease is the presence of fibrillar protein deposits, or plaques, in the brain tissue of affected individuals, most recent data suggest that nonfibrillar aggregates or oligomers formed by amyloid proteins are in fact the cytotoxic species (4–7). The link between oligomer formation and cell death is not yet understood; however, one commonly proposed mechanism for the toxicity of small, nonfibrillar amyloid assemblies is through direct interaction with the plasma membrane, leading to loss of membrane integrity and ultimately to cell death (5, 8).

There are a number of ways in which amyloid peptides can interact with the membrane. One possible mechanism of disruption is through pore formation. The potential presence of amyloid pores formed by the Alzheimer disease amyloid β (Aβ)[5] peptide has been reported by several groups (9–12), and

* This work was supported in part by the Natural Sciences and Engineering Council of Canada Discovery Grants RGPIN 342069 (to S. S.) and Yip-RGPIN 194435 (to C. M.) and an operating grant from PrioNet Canada and the Alberta Prion Research Institute (to V. S. and S. S.).
[S] This article contains supplemental Figs. 1–4.
[1] Recipient of a Natural Sciences and Engineering Council of Canada Graduate Scholarship.
[2] Supported by an Ontario graduate scholarship and a partial studentship from Restracomp (The Hospital for Sick Children).
[3] Clinical Investigator of the Alberta Heritage Foundation for Medical Research.
[4] Tier II Canada Research Chair. To whom correspondence should be addressed: Molecular Structure and Function Program, The Hospital for Sick Children, 555 University Ave., Toronto, Ontario M5G 1X8, Canada. Tel.: 416-813-7852; Fax: 416- 813-5022; E-mail: ssharpe@sickkids.ca.

[5] The abbreviations used are: Aβ, amyloid β; PrP, prion protein; AFM, atomic force microscopy; pTIRF, polarized total internal reflection fluorescence; PrP^C, cellular prion protein; POPC, 1-palmitoyl-2-oleoyl-L-phosphatidylcholine; TEM, transmission electron microscopy; LUV, large unilamellar vesicle; IAPP, islet amyloid polypeptide; PI, propidium iodide; Lo, liquid ordered; POPG, 1-palmitoyl-2-oleoyl-L-phosphatidylglycerol; DSPC, 1,2-distearoyl-phosphatidylcholine; DiI, 1,1′-dioctadecyl-3,3,3′,3′-tetramethylindocarbocyanine iodide; MTS, 3-(4,5-dimethylthiazol-2-yl)-5-(3-carboxymethoxyphenyl)-2-(4-sulfophenyl)-2*H*-tetrazolium.

similar observations have been made for other amyloid systems (13, 14). In each case, it is proposed that β-sheet-rich peptides can either form barrel-stave or toroidal pores in the membrane. The end effect of pore formation is a loss of membrane potential, as observed by single channel measurements as well as loss of solutes resulting in cell death. Interestingly, antibodies raised against pore-like annular protofibrils formed by Aβ(1–42) recognize oligomeric pores of the α-hemolysin, suggesting that there may be a common structural element (15).

It is also possible for peptides to disrupt membranes by behaving as a detergent. In this case, peptides remove lipid molecules directly resulting in bilayer destabilization. Detergent-like action by a peptide has been seen with human IAPP(20–29), where small vesicle formation was observed for a range of peptide concentrations (16). This is similar to the detergent action of membrane-destabilizing peptides through the so-called carpet model, whereby peptides aggregate on the surface of the bilayer and cause general destabilization. Both carpeting and detergent-like behavior have been reported for a number of antimicrobial peptides (17, 18) and may be a mode of action shared with amyloid oligomers.

Finally, it has been proposed that peptide fibrillization on the surface of the membrane can lead to the formation of peptide-rich microdomains inside the bilayer, causing destabilization. This may be linked to an apparent affinity of some amyloid peptides for membrane components associated with the formation of lipid rafts, such as cholesterol and glycolipids (19–21). It is well known that maintaining lipid rafts, and the membrane proteins associated with them, is very important for *in vivo* cell survival (22, 23).

PrP(106–126), a 21-residue peptide derived from the unstructured N terminus of the full-length prion protein, forms both amyloid fibrils and cytotoxic nonfibrillar oligomers (5, 24–26). Despite extensive study, the mechanism through which this peptide induces cell death has remained elusive. PrP(106–126) has been shown to be toxic both in the presence and absence of full-length PrP (27–29). It has been shown to interact with and disrupt model membranes with varied composition, with some evidence for preferential binding of raft-like membranes (30). Specific to membrane disruption by PrP(106–126) oligomers, it was shown previously that these structures directly cause membrane permeabilization (8). This peptide has also been shown to interact with L-type voltage-sensitive calcium channels (31), cause changes in membrane viscosity (32), activate the JNK-c-Jun pathway (33), form channels or pores in planar bilayers (34, 35), and be toxic to neuroblastoma cells (36).

We have previously reported the structures of both the amyloid fibrils and nonfibrillar oligomers formed by PrP(106–126) (37–39). Here, we confirm that the oligomers are cytotoxic to mammalian cells, and also demonstrate that they exhibit antimicrobial activity. AFM, TEM, and polarized TIRF (pTIRF) microscopy, in combination with ^{31}P and ^{2}H NMR spectroscopy, were used to provide mechanistic details of membrane disruption by PrP(106–126). Our data support a model in which anionic liposomes are solubilized by the peptide, leading to micellization and loss of membrane integrity. Importantly, the oligomers exhibit very different behavior when added to zwitterionic membranes containing ordered cholesterol-rich domains (mimicking a eukaryotic cell membrane). In this case, the amyloid oligomers induce a loss of domain order and phase separation, suggesting that there is a membrane or cell type dependence. Loss of domain organization has been shown to trigger pathways leading to apoptosis, suggesting an alternative mechanism through which amyloid peptides may induce cell death.

EXPERIMENTAL PROCEDURES

Peptide Synthesis and Preparation of PrP(106–126) Nonfibrillar Oligomers—The PrP(106–126) peptide (^{106}KTNMKHMAGAAAAGAVVGGLG^{126}) was obtained from the Advanced Protein Technology Centre at the Hospital for Sick Children and was purified by reverse phase HPLC using a C8 column (Vydac) as described previously (39). A control peptide containing a scrambled sequence (MVAATLGGKVGKAGMNAAHAG) was similarly prepared. PrP(106–126) oligomers were formed by dissolving peptide in hexafluoroisopropanol at 4 mg/ml and subsequent dilution to 1 mg/ml into 10 mM acetate buffer, pH 4.6. The hexafluoroisopropanol in solution was evaporated under a stream of nitrogen gas.

Formation of Large Unilamellar Vesicles (LUVs)—To form LUVs of POPC or 3:1 POPC/POPG, appropriate amounts of 25 mg/ml lipid stocks in chloroform (Avanti Polar Lipids) were measured and dried to a film under a stream of nitrogen. This film was then taken up in water at a concentration of 25 mg/ml and lyophilized to remove residual solvent. The freeze-dried lipids were then resuspended in 20 mM HEPES buffer pH 7.4 and freeze-thawed 10 times. Samples were then either used for AFM studies, extruded through a 0.1-μm filter membrane for TEM, or extruded to 0.4 μm for analysis by solid state NMR. For the formation of 1:1:1 DOPC/DSPC/cholesterol liposomes, appropriate amounts of DOPC and DSPC in chloroform were mixed with cholesterol and dried to a film. This film was resuspended in buffer as described above, and complete lipid mixing was promoted by heating to 70 °C for 20 min prior to analysis by AFM or extrusion for solid state NMR analysis.

Transmission Electron Microscopy—For TEM analysis, a 25 mg/ml suspension of freshly extruded lipids was treated with either 120 μM PrP(106–126) oligomers or 10 mM sodium acetate, pH 4.6. These samples were then diluted 500-fold, and 4 μl of the final concentration was spotted on 400 mesh continuous carbon grids, which were previously glow-discharged for 15 s at 30 mA negative discharge. Samples were adsorbed for 2 min before blotting, rinsing twice with water, and a final staining with 2% uranyl acetate for 15 s. Images were acquired using a Jeol 1011 microscope operating at a voltage of 80 keV.

Atomic Force Microscopy—Images were acquired in fluid tapping mode with a Digital Instruments (Veeco, Santa Barbara, CA) Nanoscope IIIa Multimode AFM equipped with an "E" scanner (maximum lateral scan area 14.6 × 14.6 μm), using SNL-10 short, thin tips (Veeco Probes, Camarillo, CA, and Bruker AFM Probes, Camarillo, CA). A contact/tapping mode glass fluid cell was sealed with a silicone O-ring against a freshly cleaved muscovite mica substrate. The fluid cell, having volume of ~200 μl, was fitted with separate inlet and outlet tubing to allow for the exchange of fluid during imaging. All images were collected at a resolution of 512 × 512 pixels at scan rates

between 1 and 3 Hz using tip oscillation frequencies of ~8 or 25 kHz. Image analysis was performed with Nanoscope software (version 5.12r3, Digital Instruments). Images were typically subjected to zero order flattening and second order plane fit (*x* axis) filters.

Mica surfaces were pretreated by filling the fluid cell with 10 mM HEPES containing 150 mM NaCl at pH 7.4. Supported planar bilayers were formed by injecting ~300 μl of a lipid vesicle suspension (typically composed of 100 μl of 1 mM lipid stock and 300 μl of 10 mM HEPES containing 150 mM NaCl at pH 7.4).

PrP(106–126) oligomers were diluted in acetate buffer at pH 4.6 to 7.8 and 16 μM. Approximately 300 μl was injected into the fluid cell, enough to completely replace the fluid volume of the cell. AFM images were collected until no significant changes in the bilayer were detected (~1 h). The fluid cell was flushed with at least 300 μl of 10 mM HEPES containing 150 mM NaCl at pH 7.4 and imaged for at least 30 min. Addition of peptide and subsequent wash steps were then repeated at higher peptide concentrations.

Combined Atomic Force Microscopy and Polarized Total Internal Reflection Fluorescence Microscopy (AFM-pTIRF)—A thin slice of V1 grade muscovite mica was cleaved from 2.5-cm round discs. Mica was secured to the bottom of glass Willcodish with UV-curable adhesive (Norland Optical Adhesive 63, Norland Products, Cranbury, NJ). DiI-C_{18} (Invitrogen) was added to lipid mixtures from a stock solution, giving a final concentration of 1 mol %.

For lipid mixtures containing anionic lipids, dishes were pretreated with 2 ml of 20 mM $CaCl_2$ for several minutes and subsequently removed. 100 μl of 1 mM stock lipid and 1900 μl of 10 mM HEPES containing 150 mM NaCl at pH 7.4 were added to dishes. For lipid mixtures containing lipids with transition temperatures above room temperature, dishes were incubated at ~70 °C for 20 min and subsequently allowed to cool back to room temperature. If an excessive number of vesicles were observed under TIRF illumination, 1-ml aliquots of buffer were exchanged from the dish as needed. If a continuous bilayer was not present, 100-μl aliquots of 1 mM lipid stock were exchanged for 100 μl of buffer from the dish as needed.

Images were acquired in fluid tapping mode with a Digital Instruments (Veeco) Nanoscope IIIa Bioscope AFM using SNL-10 short, thin tips (Veeco Probes and Bruker AFM Probes). The AFM head was positioned in a vertical slot above an objective-based TIRF system. AFM image analysis was performed with Nanoscope software (Version 5.30r3, Digital Instruments). AFM images were typically subjected to zero order flattening and second order plane fit (*x* axis) filters.

A home-built pTIRF microscope built around an Olympus IX70 inverted microscope that accommodates multiple excitation laser lines was utilized for pTIRF microscopy (40). The bottom of the dish was brought into focus under ambient lighting under oil immersion using a ×60 1.45 NA TIRF objective. Appropriate filters were then inserted, and a region of the supported bilayer was brought into focus under pTIRF illumination. Images were captured with an Evolve 512 EMCCD camera (Photometrics, Tucson, AZ) controlled by Micro-Manager. Fluorescent probes were excited by parallel or perpendicular polarized light, relative to the substrate surface, through the rotation of a half-wave plate in the excitation path.

Solid State NMR—Solid state NMR experiments were carried out using a Varian VNMRS spectrometer operating at a ^{1}H frequency of 499.71 MHz. Static ^{31}P and ^{2}H NMR spectra were acquired using a 3.2-mm T3 MAS probe. ^{31}P and ^{2}H $\pi/2$ pulse widths were 4.5 and 2.5 μs, respectively. 50 kHz ^{1}H decoupling was used during the acquisition of ^{31}P spectra. ^{2}H spectra were acquired using a quadrupolar echo pulse sequence, with an echo delay of 40 μs. All spectra were processed using NMRPipe and visualized in nmrDraw.

Antimicrobial Activity Assay—Escherichia coli BL21 cells (Invitrogen) were grown overnight at 37 °C in 50 ml of Luria Broth (LB) without antibiotics. Cells were diluted in LB to reach an absorbance of 0.03 at 600 nm. A 96-well plate was used to set up the experimental conditions in triplicate with each condition having a volume of 50 μl before the addition of 200 μl of cell suspension (250 μl total volume). As a negative control, 1 mg/ml carbenicillin (final concentration) was used. Blanks were set up in triplicate for each condition to account for the dilution of the LB by acetate and Tris buffers. After setting up the plate, an initial absorbance reading at 650 nm was recorded after which the 96-well plate was placed in a 37 °C incubator and removed at 30, 120, 180, 240, and 300 min for absorbance readings.

Cell Culture—PC12 cells were cultured in F12K nutrient media with 10% horse serum, 5% FBS, penicillin, streptomycin, glucose, and sodium pyruvate; N2a and SHSY-5Y cells were cultured in DMEM high glucose supplemented with 5% FBS, penicillin, streptomycin, glucose, and sodium pyruvate. Two N2a subclones were tested, with different PrP^{C} expression levels (subclone 2 has ~2× more PrP^{C} than subclone 1, by Western blot analysis). Cells were plated in collagen-coated 96-well plates. At 75% confluence, media were replaced with 90 μl of low serum media, containing 1% total serum (FBS). 10 μl of 10× treatment (fibrils, oligomers, or scrambled peptide) was added to each well for final concentrations of 5, 10, 50, or 100 μM. 10 μl of fibril and oligomer buffer were used as negative controls, whereas 5 μM staurosporine was used as a positive control. At 8 and 24 h after treatment, 20-μl aliquots were removed from each well and assayed for adenylate cyclase release using the Toxilight assay (Lonza) according to the manufacturer's instructions. At 48 h, wells were assayed for viability using the 3-(4,5-dimethylthiazol-2-yl)-5-(3-carboxymethoxyphenyl)-2-(4-sulfophenyl)-2*H*-tetrazolium (MTS) reduction assay (Promega) according to the manufacturer's instructions. Statistical analysis was carried out using a standard Z-test.

Mouse Cerebellar Slice Organotypic Cultures—Cerebellar slice cultures were prepared from 10- to 12-day-old C57B16 mice as described by Falsig and Aguzzi (41). Slices were cultured for 14 days prior to treatment to allow cultures to stabilize. After treatment with oligomers or controls, slices were treated with 200 μl of warm slice medium containing 10 μg/ml propidium iodide (PI) (Invitrogen) for 15 min and then washed three times with 500 μl of PBS, pH 7.4, to remove residual PI. Incubations and washes were done in the dark. Next, the slices were fixed with fresh 4% paraformaldehyde (Invitrogen) in PBS for 15 min and then washed three times with 500 μl of PBS.

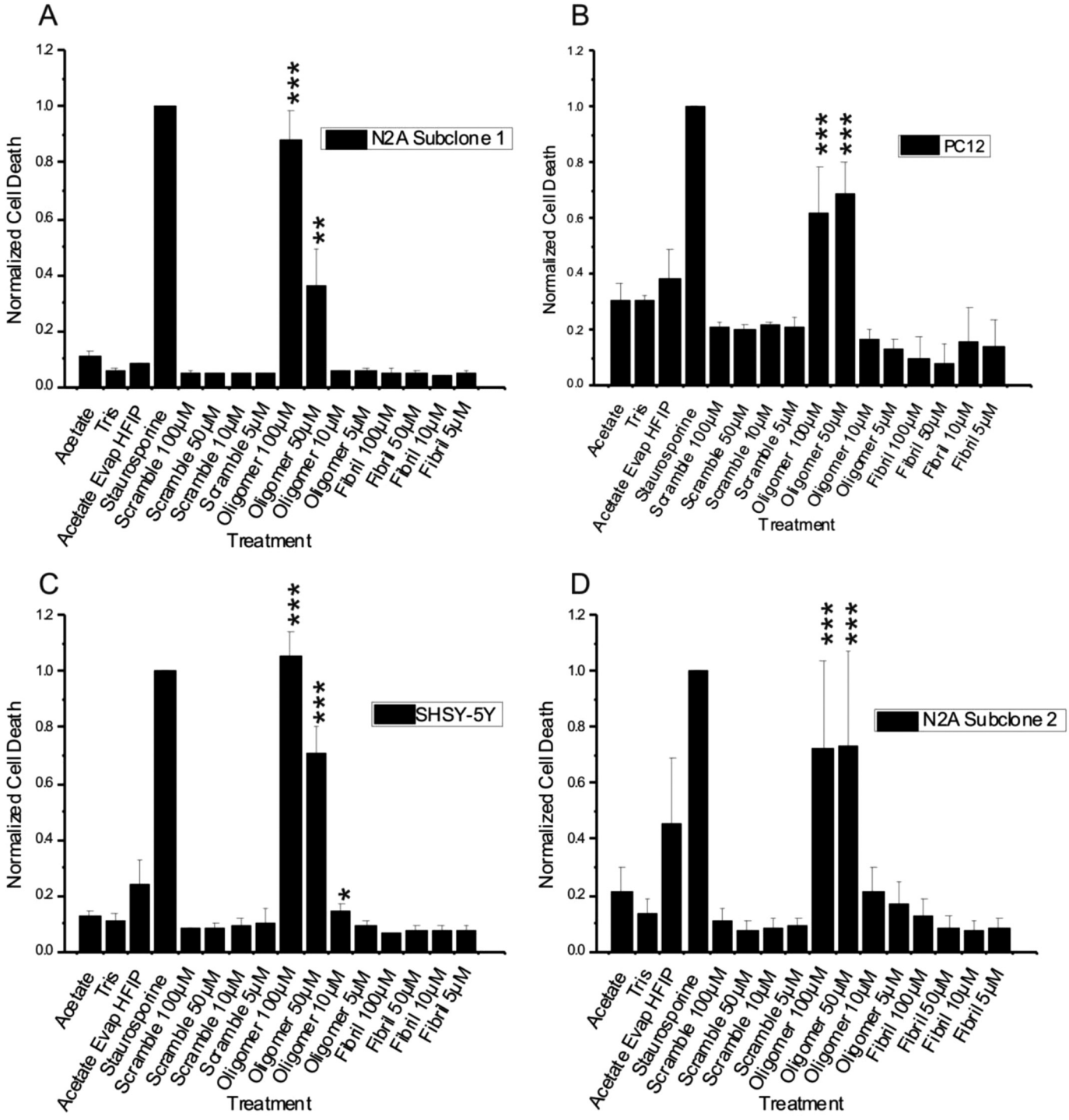

FIGURE 1. **Cytotoxicity of PrP(106–126) oligomers in mammalian cell culture.** Normalized cell death, as monitored using the Toxilight assay, is shown for N2a (subclone 1) (*A*), PC12 (*B*), SHSY-5Y (*C*), and N2a (subclone 2, 2× more PrP^C) (*D*) cells treated with 5–100 μM PrP(106–126) oligomers, fibrils, or a scrambled control peptide for 24 h. 5 μM staurosporine was used as a positive control, whereas 10 μl of fibril and oligomer buffers (acetate, acetate with hexafluoroisopropanol, and Tris) were added as negative controls. In all cell types, 100 and 50 μM PrP(106–126) was able to produce statistically significant cell death *versus* buffer alone (***, corresponding to $p < 0.01$; **, $p < 0.03$, and *, $p < 0.05$). The fraction of dead cells was normalized in each case against the positive control staurosporine. *Error bars* represent the standard deviation of measurements made in triplicate.

Slices were permeabilized with 0.25% Triton X-100 in PBS for 15 min and then washed three times with 500 μl of PBS. Slices were blocked using 1% goat serum, 1% BSA in PBS for 1 h, labeled with 1:4000 dilution of anti-mouse calbindin (Abcam) in blocking buffer for 1 h, washed three times with 500 μl of PBS, labeled with 1:4000 anti-goat Alexa Fluor 488 secondary (Invitrogen) for 30 min, then washed three times with 500 μl of PBS. The membrane supporting the slices was then removed from the insert support and placed on a slide, tissue side up. Three drops of Prolong Gold with 4′,6-diamidino-2-phenylindole (DAPI) (Invitrogen) were placed on the membrane insert, and a coverslip was affixed to the slide. Slides were cured for a

minimum of 24 h. Determination of slice viability (PI staining) was done from images taken at Nyquist resolution sampling on a Zeiss LSM 700. Images were first deconvolved using ImageQuant X, and analysis was completed using Imaris 7.1.1 software. Percent cell death was calculated as the number of PI-positive cells divided by the number of DAPI-positive cells.

RESULTS

PrP(106–126) Oligomers Are Cytotoxic to Eukaryotic Cells and Inhibit Bacterial Growth—To confirm the reported toxicity of PrP(106–126) oligomers, and to assess the activity of our samples, we treated four different mammalian cell lines with PrP(106–126) oligomers, fibrils, and a scrambled peptide. As shown in Fig. 1, PrP(106–126) oligomers caused a significant increase in the death of N2a subclones 1 and 2, PC-12, and SH-SY5Y cells, as monitored using the Toxilight assay after 24 h of incubation. This colorimetric assay uses the release of adenylate kinase from cells as an indicator of cell damage or death (42). In all cases, 100 μM PrP(106–126) oligomers exhibited a level of cytotoxicity similar to 5 μM staurosporine, which is known to initiate apoptosis in a wide range of cell types (43). Amyloid fibrils and nonoligomerizing scrambled PrP(106–126) peptide did not exhibit significant toxicity to the tested cell types. A similar effect was observed as early as 8 h (supplemental Fig. S1), and these results were confirmed using MTS reduction as a second assay for cell death (supplemental Fig. S2).

In addition to exhibiting cytotoxicity in mammalian cell culture, PrP(106–126) oligomers also caused significant cell death in cultured mouse cerebellar slices (supplemental Fig. S3). At 24 and 48 h post-treatment with 100 μM oligomeric PrP(106–126), a large increase in PI fluorescence was observed, indicating loss of membrane integrity allowing PI to enter the nucleus and bind DNA (44). By 24 h, 55% of the cell nuclei had incorporated PI, while at 48 h post-treatment 61% of mouse cerebellar cells had died.

The amino acid composition of PrP(106–126) is reminiscent of cationic antimicrobial peptides, particularly dermaseptin (45). Importantly, many cationic antimicrobial peptides have hemolytic activity, such that they kill both prokaryotic and eukaryotic cells, presumably through direct membrane disruption (17, 18). To test the possibility that PrP(106–126) may act through a mechanism similar to cationic antimicrobial peptides, we performed a bacterial inhibition assay. As shown in Fig. 2, oligomeric PrP(106–126) inhibited the growth of BL21 *E. coli* cultures in a concentration-dependent manner, although fibrillar peptide did not.

PrP(106–126) Oligomers Disrupt Anionic Lipid Bilayers—To determine whether membrane disruption forms the physical basis for PrP(106–126) cytotoxicity, *in vitro* studies were carried out using highly simplified models of bacterial and mammalian membranes. A POPC/POPG lipid mixture has been used by several groups as a mimic of anionic bacterial membranes (46, 47). We have previously reported disruption of liposomes with this composition by PrP(106–126), using leakage of the fluorescent dye calcein as a readout (48), and here we use 3:1 POPC/POPG bilayers to probe the mechanism of antimicrobial activity.

Supported POPC/POPG bilayers were imaged using tapping mode AFM in solution at room temperature. As expected for this binary mixture, which has a fluid to gel phase transition

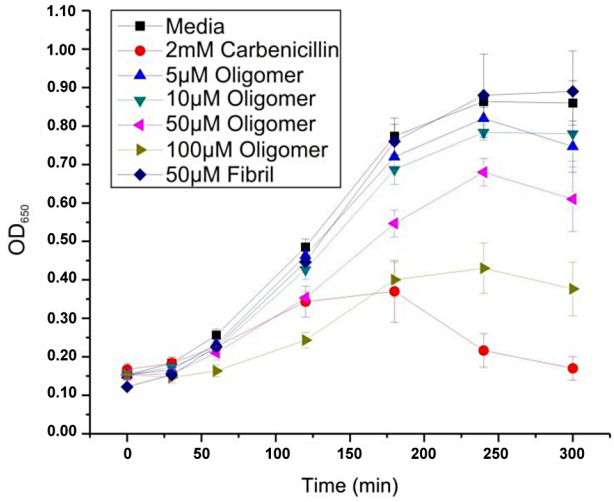

FIGURE 2. **Antimicrobial activity of PrP(106–126) oligomers.** The A_{650} values recorded for *E. coli* (BL21) cultures at several time intervals are shown. Bacterial cultures were diluted to a starting A_{650} of 0.1 and then grown in the presence of 5–100 μM PrP(106–126) oligomers (*triangles*), 50 μM PrP(106–126) fibrils (*diamonds*), or media alone (*squares*). Oligomers show a dose-dependent reduction in cell growth, approaching that of the antibiotic carbenicillin (*circles*), whereas fibrils and blank media do not inhibit growth. *Error bars* represent the standard deviation of measurements made in triplicate.

temperature of approximately −2 °C, a molecularly smooth surface populated with some small unfused vesicles was observed (Fig. 3). Upon addition of PrP(106–126) oligomers, raised structures extending ~4.5 nm above the bilayer surface were observed. These structures are consistent with the peptide-induced formation of vesicles, which is a phenomenon previously observed after the interaction of IAPP with liposomes (16) and Aβ(1–40) with supported bilayers (49). After washing with excess buffer, the bilayer was depleted at locations previously exhibiting increased height profiles, giving rise to ~5–6-nm deep defects. This is approximately the thickness reported for Lα POPC bilayers (inclusive of hydration shell) (50, 51) and is also suggestive of vesicles being removed from the bilayer after treatment with PrP(106–126). Further evidence for the formation of small vesicles or micelles was provided by TEM images of 3:1 POPC/POPG LUVs (Fig. 4). Although initially appearing spherical and smooth, upon addition of PrP(106–126) oligomers the surface of the LUVs became irregular and populated by small protrusions.

To examine the changes in the bilayer at the molecular level, static ^{31}P NMR spectra were obtained for 400 nm LUVs. In the absence of peptide, a powder pattern is observed for 3:1 POPC/POPG LUVs (Fig. 5*A*). This spectrum exhibits the characteristic line shape and line width (53 ppm) of Lα phase bilayer membranes (52). Upon addition of 120 μM PrP(106–126) oligomers, there is a marked reduction in line width, with the resulting spectrum having a significantly narrower peak (~5 ppm) centered around the ^{31}P isotropic chemical shift. This reduction in line width results from an averaging or reduction in the ^{31}P chemical shift anisotropy and can be attributed to either a dramatic reduction in the order parameter of the bilayer or to the large scale release of small, fast tumbling vesicles from the larger 400 nm LUVs. The latter phenomenon has been reported for some amyloids, most notably IAPP (16), and other membrane disrupting peptides such as MSI-78 (53).

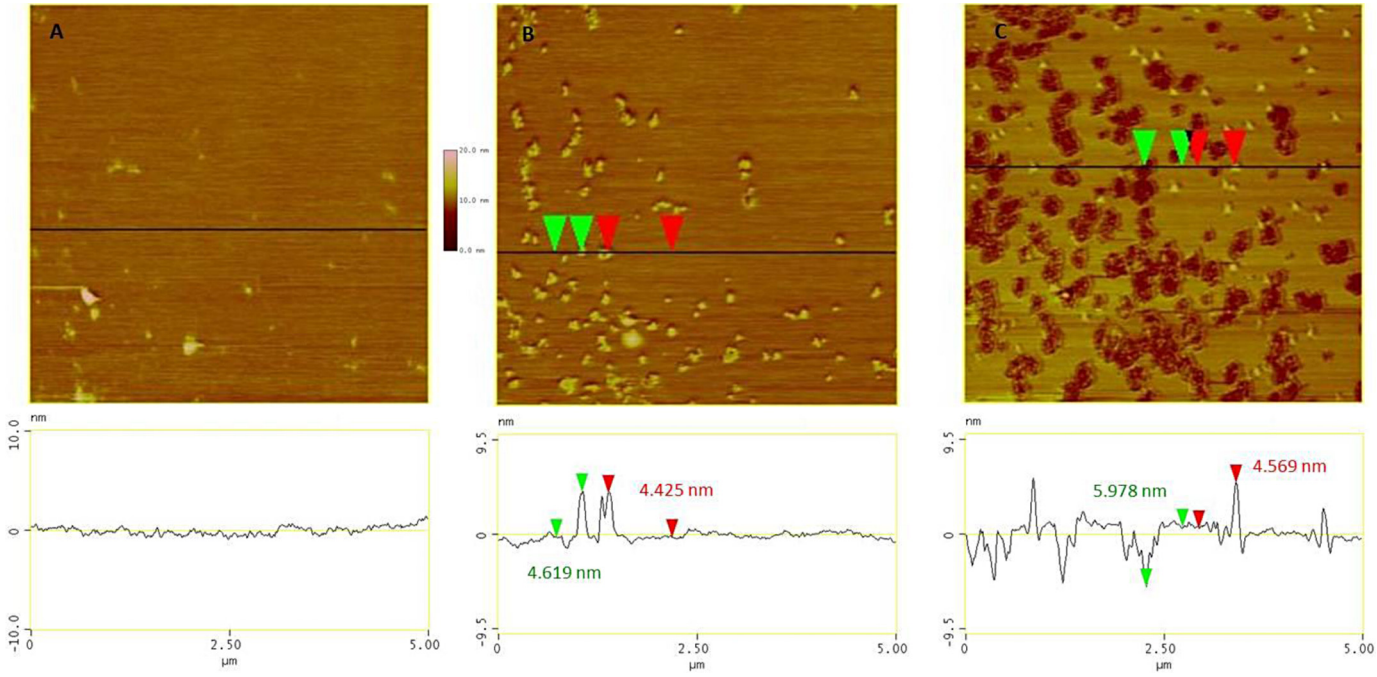

FIGURE 3. **AFM images of 3:1 POPC/POPG supported bilayers in the presence and absence of PrP(106–126) oligomers.** Height images from tapping mode AFM of supported 3:1 POPC/POPG bilayers are shown. *A,* initial lipid bilayer is relatively flat, but after addition of 0.015 mg/ml peptide solution (*B*), raised features ~4.5 nm in height are apparent above the bilayer surface. *C,* after subsequent washing with HEPES pH 7.4 buffer, holes or defects with a depth of 5–6 nm appear in the bilayer, corresponding to the approximate thickness reported for a single hydrated Lα phase POPC bilayer. Each AFM image represents the same 5 × 5 μm area of the supported bilayer. The *traces* below each image show the height profile taken along the *horizontal black lines*.

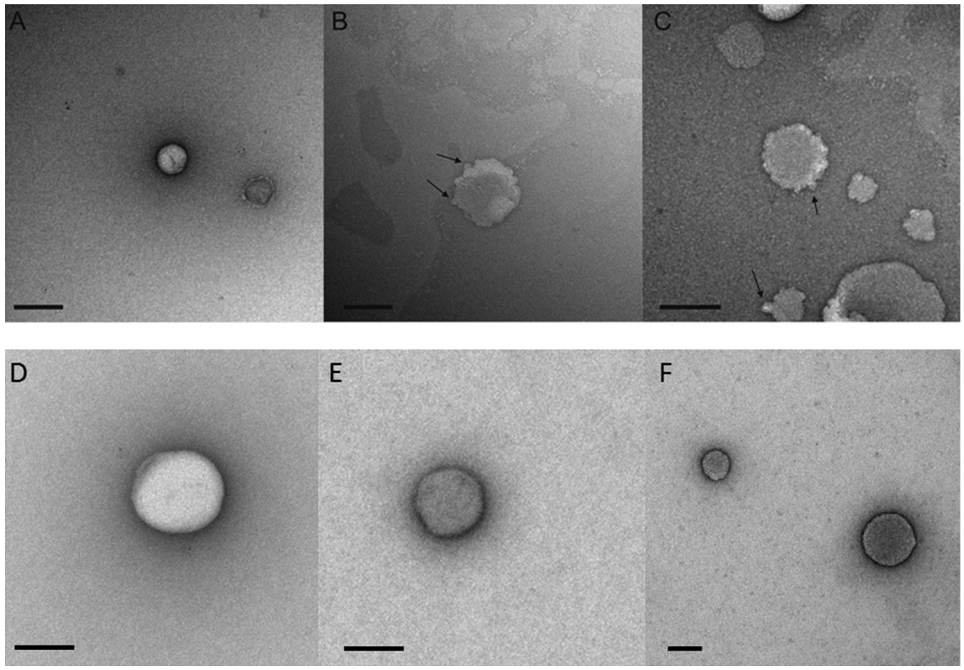

FIGURE 4. **Negative stain TEM images of LUVs in the presence and absence of PrP(106–126) oligomers.** TEM images are shown for uranyl acetate-stained liposomes formed from 3:1 POPC/POPG (*A–C*) and 1:1:1 DOPC/DSPC/cholesterol (*D–F*). *A,* untreated POPC/POPG LUVs appear as nearly spherical shapes with round edges. *B,* after addition of 120 μM PrP(106–126) oligomers, surface blebbing can be seen (*arrows*). *C,* additional view shows multiple LUVs with surface disruptions, suggesting the release of small vesicles from the surface of the LUV (*arrows*). The presence of larger liposomes is also apparent. By contrast, no change in liposome morphology is observed for DOPC/DSPC/cholesterol liposomes in the absence (*D*) or presence (*E* and *F*) of PrP(106–126) oligomers. The *scale bar* in each image represents 100 nm.

PrP(106–126) Oligomers Cause Altered Domain Organization and a Reduction in Order of Cholesterol-containing Bilayers—As a simplified model of mammalian cell membrane organization, liposomes composed of 1:1:1 DOPC/DSPC/cholesterol were used. This ternary mixture has been shown to form biphasic bilayers with DOPC-rich Lα domains coexisting with more rigid liquid ordered (Lo) domains enriched in DSPC and cholesterol (54, 55). As such, it is a useful model system for

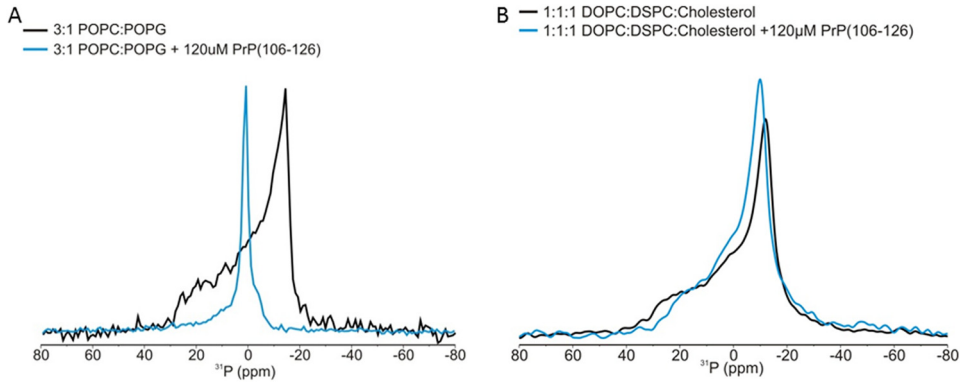

FIGURE 5. **Static ^{31}P NMR spectra of LUVs in the presence and absence of PrP(106–126) oligomers.** ^{31}P NMR spectra are shown for 3:1 POPC/POPG (*A*) or 1:1:1 DOPC/DSPC/cholesterol (*B*) LUVs before addition of peptide (*black*) and after treatment with 120 μM PrP(106–126) oligomers (*blue*). Spectra were recorded at 21 °C.

investigating lipid microdomains. This is of potential importance when examining the effects of amyloid oligomers on membranes, because there is a wealth of data linking cholesterol-rich domains with amyloid binding and with cell death associated with amyloidosis (19, 56–58).

Combined AFM-pTIRF microscopy images of supported DOPC/DSPC/cholesterol bilayers containing 1 mol % DiI-C_{18} are shown in Fig. 6*A*. These data were acquired at room temperature in solution, facilitating study of the membrane under near native conditions. The AFM image clearly shows the presence of both Lα and raised Lo domains. Confirmation of this domain separation and a means to monitor the order of the membrane were obtained using pTIRF microscopy of the same section of bilayer. As we have shown, the observed intensity of the fluorescent emission of DiI-C_{18} when excited with polarized light will depend on both the orientation of the polarization (perpendicular or parallel) and the local order (40, 54, 59–61). DiI-C_{18} is also known to exhibit preferential partitioning into ordered lipid phases, making it an excellent probe of domain formation and changes in bilayer order (54, 62, 63).

As can be seen in the *middle panels* of Fig. 6*A*, regions of high intensity fluorescence are observed under excitation with parallel light (F_s). These correspond to the ordered cholesterol-rich domains identified using AFM. Similar but weaker fluorescence was observed after excitation with perpendicularly polarized light (F_p).

The order parameter $\langle P_2 \rangle$ was calculated for each pixel, using the difference in F_s and F_p fluorescence emission intensity (see under "Experimental Procedures"), and an image color-coded by order parameter is shown in the *right-hand panel* of Fig. 6*A*. This orientational order parameter ranges from −0.5 to 1, with the extremes representing single orientations of the fluorophore, and all other values indicating the presence of a distribution of molecular orientations.

The effect of PrP(106–126) oligomers on 1:1:1 DOPC/DSPC/cholesterol bilayers as monitored by AFM is shown in Fig. 7. As in Fig. 6*A*, clear separation of the Lα and Lo domains is evident prior to addition of peptide. After addition of peptide oligomers, domain separation is lost, and amyloid fibrils can be observed on the surface of the membrane. No visible holes or defects are apparent in these images, in contrast to the effect of PrP(106–126) on anionic bilayers (Fig. 3). TEM images of DOPC/DSPC/cholesterol LUVs (Fig. 4) support this observation, as no alterations in liposome morphology are observed for this bilayer composition in the presence of PrP(106–126) oligomers.

The loss of domain organization was supported by pTIRF microscopy images of a similar bilayer (Fig. 6*B*). Prior to the addition of peptide (Fig. 6*B*, *0 min*), the presence of higher order lipid domains is evident. At longer incubation times, there is a clear loss of domain separation, with DiI-C_{18} fluorescence spreading through the membrane. Time-lapse video of this process (supplemental Fig. S4) indicates that the changes begin from within the ordered domains and spread outward, suggesting that these may represent the initial sites of peptide binding.

As is evident in the color-coded $\langle P_2 \rangle$ images shown in Fig. 6*B*, there is a change in the orientational order of the DiI-C_{18} after incubation of the membrane with PrP(106–126) oligomers, as well as a gradual reduction in domain separation. As the histograms summarizing the information from each image show, there is both a broadening of the distribution of $\langle P_2 \rangle$ values after incubation with the peptide oligomers within the images and an overall decrease in the mean value of $\langle P_2 \rangle$ by 16–17%. These pTIRF data support the loss of ordered domain separation, as well as a decrease in the global order parameter of the bilayer.

The ^{31}P NMR spectra of DOPC/DSPC/cholesterol liposomes (Fig. 5*B*) show that the bilayer nature of is not significantly altered by the addition of PrP(106–126) oligomers. Instead, there is a slight reduction in the breadth of the static powder pattern (15–20%), consistent with the change in the global order parameter as measured by pTIRF. The absence of narrow or isotropic components indicates that no micellization or large scale disruption of the bilayer has occurred.

Further support for reduced membrane order was obtained using ^{2}H NMR spectroscopy to directly probe mobility and order of cholesterol within the membrane. Static ^{2}H NMR spectra of DOPC/DSPC/cholesterol LUVs containing 3-d_1-cholesterol (single ^{2}H label at the 3-position) are shown in Fig. 8. The quadupolar coupling constant for this ^{2}H-C group in PC membranes has been previously measured as 44 kHz at 20 °C (64). In the absence of peptide, we observe a ^{2}H quadrupolar splitting of 47.9 kHz at 21 °C, consistent with partitioning into Lo phase DSPC-cholesterol enriched domains. As the sample temperature approaches (65 °C) and exceeds (75 °C) the phase

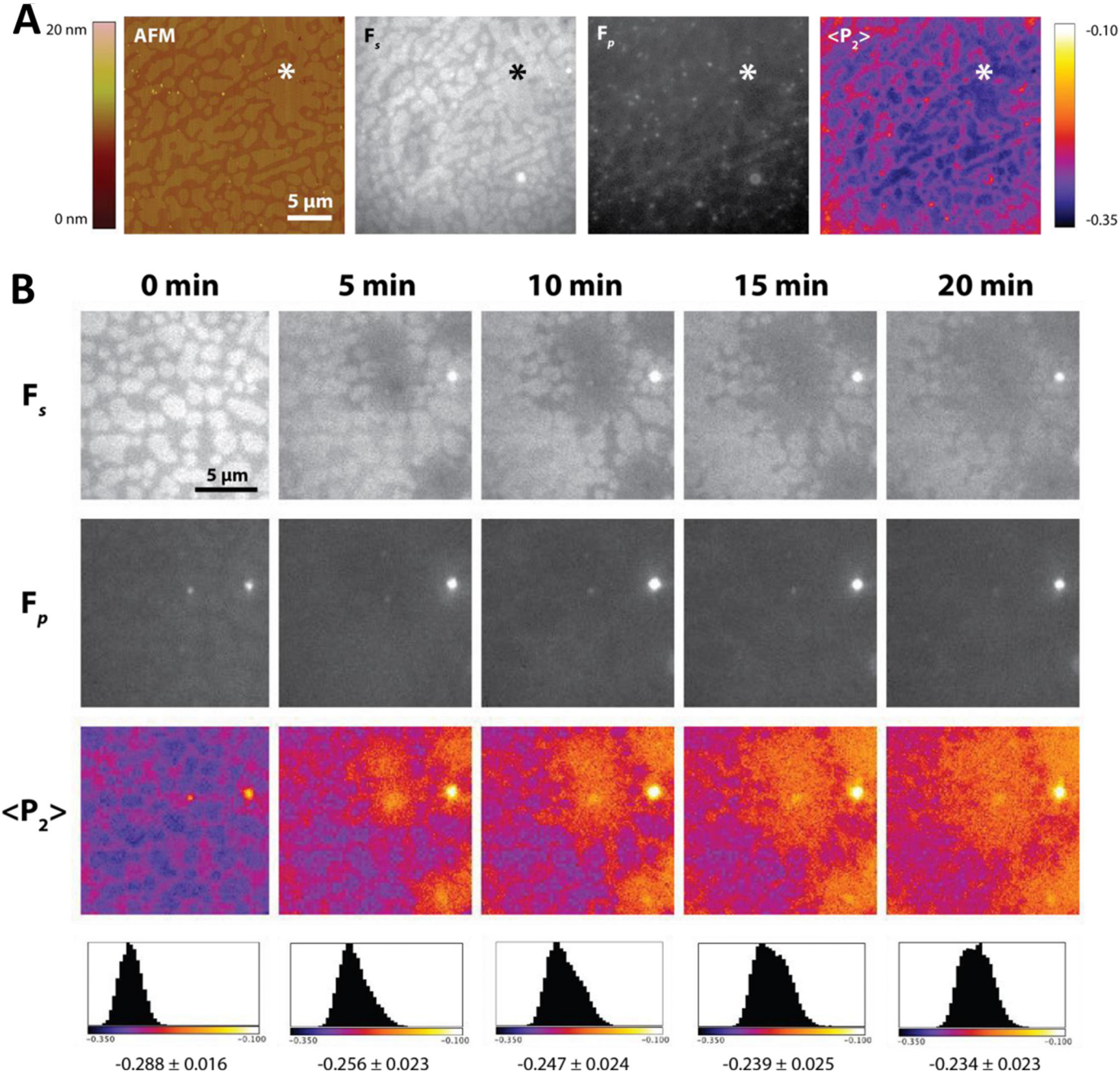

FIGURE 6. **AFM and polarized TIRF microscopy of supported bilayers formed by 1:1:1 DOPC/DSPC/cholesterol.** *A,* combined AFM and pTIRF images are shown for a 30 × 30 μm region of a DOPC/DSPC/cholesterol bilayer in the absence of peptide. The *left panel* shows a height image obtained using tapping mode AFM of a supported lipid bilayer. Polarized TIRF images obtained using parallel excitation (F_s) or perpendicular excitation (F_p) of the fluorescent probe DiI-C_{18}, incorporated at 1 mol % relative to lipid, are shown for the same region of the bilayer (*center panels*). The *right-hand panel* shows the same image colored by the order parameter $\langle P_2 \rangle$, calculated as described in the text. Each image shows the same area, and a reference spot is indicated in each panel (*). *B,* F_s- and F_p-polarized TIRF images are shown for several time points following the addition of PrP(106–126) oligomers to a supported bilayer at a final concentration of 4.1 μM. The intensely *bright dots* in each panel are due to the presence of a vesicle within the pTIRF illumination field. The $\langle P_2 \rangle$ panels correspond to each pair of fluorescence micrographs, and the range of observed order parameters within each image is summarized as a histogram in the *bottom panel* for each time point, with the mean value indicated in each case. Each image represents the same 15 × 15 μm area of the bilayer.

transition temperature of DSPC, domain separation is lost, and the ^{2}H spectrum collapses to 2.7 kHz due to increased mobility of the cholesterol and the concurrent reduction in the order of the bilayer.

In the presence of peptide, there is a small reduction in the width of the ^{2}H powder spectrum and an increased isotropic component, similar to the effect of increasing temperature in the absence of peptide. Although the bilayer does not appear to undergo a whole scale perturbation, it is clear that the cholesterol is now experiencing a less ordered environment, as suggested by the pTIRF and ^{31}P NMR data.

DISCUSSION

The formation of nonfibrillar oligomers has been clearly identified as a key event during the misfolding of amyloid proteins, and these entities have been implicated as the cytotoxic

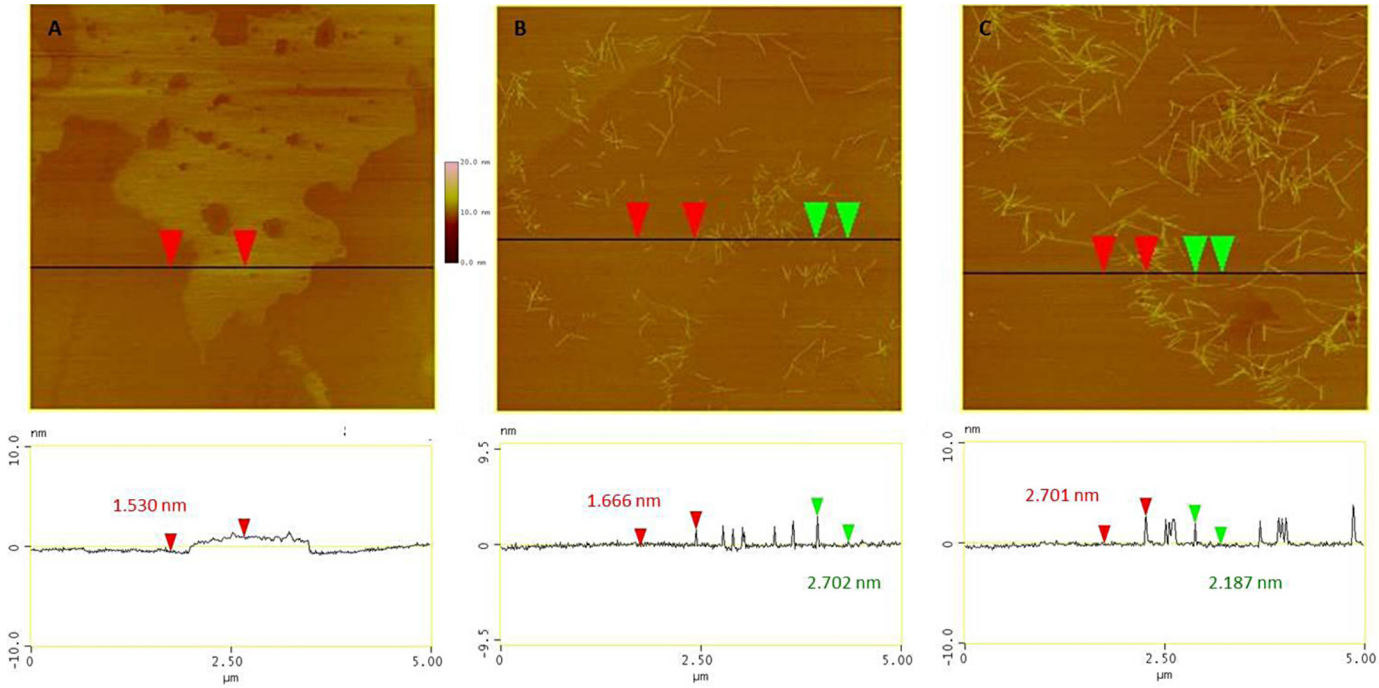

FIGURE 7. **AFM images of 1:1:1 DOPC/DSPC/cholesterol-supported bilayers in the presence and absence of PrP(106–126) oligomers.** Height images from tapping mode AFM of supported DOPC/DSPC/cholesterol bilayers are shown. *A,* prior to the addition of peptide, two domains with a 1.5-nm height difference are observed. *B,* after addition of 0.015 mg/ml peptide oligomers, no phase separation is visible, and amyloid fibrils appear on the surface. *C,* after addition of 0.04 mg/ml peptide oligomers, a higher density of longer fibrils is observed. All images show a 5 × 5 μm area. The *traces* below each image show the height trace along the indicated slice, with selected height differences indicted by *red* and *green arrows*.

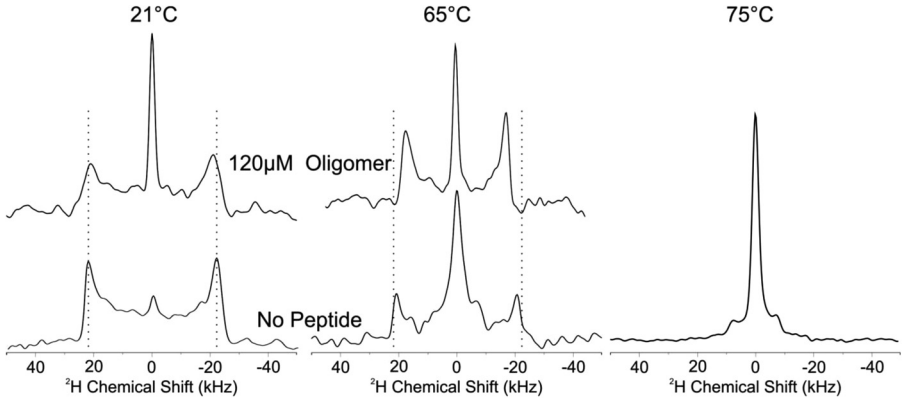

FIGURE 8. **^{2}H NMR spectra of 1:1:1 DOPC/DSPC/(3-d_1-cholesterol).** Static ^{2}H NMR spectra are shown for 400-μm liposomes formed from 1:1:1 DOPC/DSPC/cholesterol, with the cholesterol labeled by a single deuteron at position 3. Spectra were acquired at 21, 65, and 75 °C in the absence of peptide (*bottom*) as well as at 21 and 65 °C after the addition of 120 μM peptide (*upper*). The *dashed vertical lines* indicate the quadrupolar splitting observed at 21 °C without peptide.

forms of amyloid proteins. Regarding the pathway through which amyloid oligomers cause cell death, several possibilities have been proposed, including oligomer binding to specific cell-surface proteins or receptors leading to altered cell signaling or channel activity or through direct perturbation of the cell membrane (7, 13, 65). Substantial evidence for the latter has been reported for several amyloid proteins and peptides, although the physical basis for the disruption remains in question. It has also been proposed that there might be a common mechanism for the cytotoxicity of different amyloid proteins, largely based on morphological and structural similarities between nonfibrillar oligomers formed by different proteins (5, 7, 8).

Induction of apoptosis by PrP(106–126) has previously been reported by several groups (31, 66, 67), and the proposed mechanisms range from formation of pores or channels (8, 68) to increased membrane microviscosity (31, 32, 66, 67). Consistent with previous reports (5), we observe specific cytotoxicity of only the oligomeric state of PrP(106–126). These oligomers induce cell death in mouse, human, and rat neuronal cell cultures as well as in mouse cerebellar tissue. In the latter system, we did not discern any cell type specificity, suggesting that the oligomers act through a nonspecific mechanism to induce cell death. Likewise, the ability to kill eukaryotic cells and to inhibit the growth of bacterial culture suggests that PrP(106–126) toxicity does not necessarily require a specific cell-surface receptor but can act through direct physical association and perturbation of cell membranes. Although some evidence suggests that PrP(106–126) toxicity may require the presence of PrP^C on the cell surface (69–71), our data support a PrP^C-independent

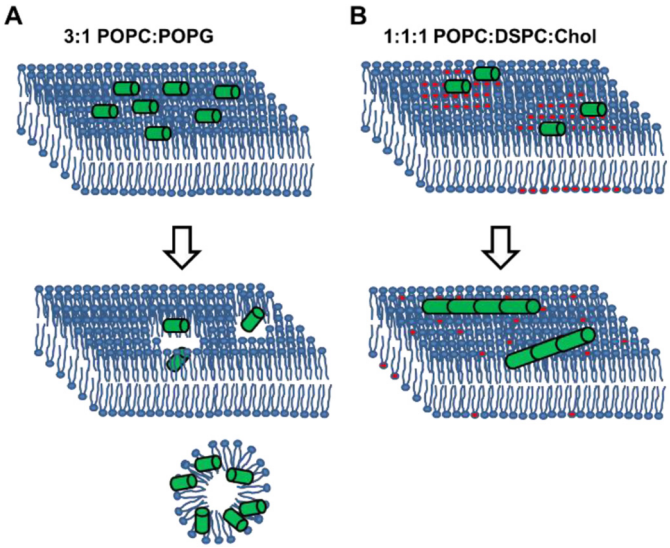

FIGURE 9. **Models of membrane perturbation by PrP(106–126) oligomers.** *A,* addition of peptide oligomers (*green*) to POPC/POPG membranes results in physical removal of peptide-lipid micelles, causing membrane leakage and cell death. *B,* addition of PrP(106–126) oligomers to membranes containing ordered cholesterol-rich domains (indicated by *red* DSPC headgroups) results in fibril assembly on the membrane surface concurrent with a loss of domain organization. Based on our pTIRF data, we propose that peptide binding initially occurs preferentially within the ordered lipid domains and that domain reorganization subsequently spreads from the initial sites of peptide association.

pathway (29). Use of a cell line with 2× the cell surface PrP^C (N2a subclone 2) did not significantly increase PrP(106–126)-induced cell death.

Our data provide evidence that a single type of oligomer formed by one peptide may act to disrupt membrane integrity through multiple distinct mechanisms, dependent on the composition of the bilayer. A schematic outlining our proposed models for membrane disruption by PrP(106–126) is shown in Fig. 9. Fig. 9*A* depicts disruption of anionic membranes by PrP(106–126) oligomers through a modified carpet model, similar to the mode of action proposed for some cationic antimicrobial peptides (17, 18). Based on our TEM, AFM, and ^{31}P NMR data, binding of the oligomeric peptide to the membrane is followed by extraction of small vesicles or micelles, leaving defects in the bilayer and resulting in bacterial cell death.

This solubilization of anionic membranes to produce mixed peptide-lipid micelles or small vesicles is similar to previously reported fragmentation of 1,2-dimyristoyl-phosphatidylcholine (DMPC) nanotubes by IAPP (72). In that work, the appearance of an isotropic peak in the lipid ^{31}P spectrum was linked to peptide-lipid small vesicle formation. More recently, it has been shown that perturbation of anionic membranes by IAPP proceeds through a similar mechanism (16). These data support recent reports of antimicrobial activity from other amyloid peptides, suggesting this may be a more general phenomenon (73).

By contrast, our biophysical data do not suggest the creation of defects or holes in zwitterionic membranes by PrP(106–126) oligomers. Instead, we propose the model shown in Fig. 9*B*. Oligomer binding to cholesterol-rich domains leads to altered lipid organization within the bilayer *in vitro*, reducing the order parameter of the membrane, a phenomenon that could cause a loss of ordered domain structure *in vivo*. This is consistent with fibril formation on the membrane surface, as observed by AFM (Fig. 7).

Despite some controversy surrounding their existence (74), the presence of ordered (Lo) cholesterol-rich lipid domains in cell membranes has been strongly supported by several recent studies (75, 76). Such microdomains may play essential roles in the spatial organization and localization of plasma membrane components. A loss of domain separation would significantly impact signaling and other cell surface-linked pathways, potentially leading to initiation of apoptosis. Disruption of lipid domains has recently been exploited in cancer therapy, as a means of initiating tumor cell death, lending support to this hypothesis (77).

Our proposal that the disruption of cholesterol domains may underlie PrP(106–126)-induced cytotoxicity fits well with earlier data showing interaction of PrP(106–126) with the ganglioside GM1, another component of lipid microdomains or rafts (18, 47). Although we have not yet examined the interaction of PrP(106–126) oligomers with GM1-containing bilayers, this peptide is clearly able to bind and disrupt ordered lipid domains in a nonganglioside-dependent manner.

Interestingly, it has been previously suggested that cholesterol may be protective against membrane disruption by amyloid oligomers of Aβ(1–42) by preventing oligomers of this peptide from sequestering GM1 at the cell surface (78). Similar results were reported for the yeast prion protein Sup35, in which fibrils binding to GM1 on the surface of live cells were able to induce caspase activity due to the rearrangement of cell-surface Fas (79). These results further demonstrate the importance of ordered lipid domains in amyloid cytotoxicity, although amyloid-induced domain reorganization has not previously been demonstrated to our knowledge.

As a final note, the observation that a single entity can induce membrane disruption through very different mechanisms dependent on bilayer composition has important implications for *in vitro* studies of amyloid toxicity. For example, model membranes formed by POPC (80), 1,2-dioleyl-phosphatidylglycerol (DOPG) (81), and 1,2-dimyristoyl-phosphatidylglycerol/1,2-dimyristoyl-phosphatidylcholine (DMPG/DMPC) (82), among many other lipid mixtures, have frequently been used to study membrane interactions of amyloid proteins and peptides. It is evident that caution must be used in selecting model membranes for such studies because the choice of lipid composition may have an unanticipated impact on experimental results.

REFERENCES

1. Glenner, G. G., and Wong, C. W. (1984) Alzheimer's disease: initial report of the purification and characterization of a novel cerebrovascular amyloid protein. *Biochem. Biophys. Res. Commun.* **120,** 885–890
2. Prusiner, S. B. (1982) Novel proteinaceous infectious particles cause scrapie. *Science* **216,** 136–144
3. Spillantini, M. G., Schmidt, M. L., Lee, V. M., Trojanowski, J. Q., Jakes, R., and Goedert, M. (1997) α-Synuclein in Lewy bodies. *Nature* **388,** 839–840
4. Baglioni, S., Casamenti, F., Bucciantini, M., Luheshi, L. M., Taddei, N., Chiti, F., Dobson, C. M., and Stefani, M. (2006) Prefibrillar amyloid aggregates could be generic toxins in higher organisms. *J. Neurosci.* **26,** 8160–8167
5. Kayed, R., Head, E., Thompson, J. L., McIntire, T. M., Milton, S. C., Cot-

man, C. W., and Glabe, C. G. (2003) Common structure of soluble amyloid oligomers implies common mechanism of pathogenesis. *Science* **300,** 486–489
6. Lambert, M. P., Barlow, A. K., Chromy, B. A., Edwards, C., Freed, R., Liosatos, M., Morgan, T. E., Rozovsky, I., Trommer, B., Viola, K. L., Wals, P., Zhang, C., Finch, C. E., Krafft, G. A., and Klein, W. L. (1998) Diffusible, nonfibrillar ligands derived from Aβ1–42 are potent central nervous system neurotoxins. *Proc. Natl. Acad. Sci. U.S.A.* **95,** 6448–6453
7. Walsh, D. M., and Selkoe, D. J. (2004) Oligomers on the brain: the emerging role of soluble protein aggregates in neurodegeneration. *Protein Pept. Lett.* **11,** 213–228
8. Kayed, R., Sokolov, Y., Edmonds, B., McIntire, T. M., Milton, S. C., Hall, J. E., and Glabe, C. G. (2004) Permeabilization of lipid bilayers is a common conformation-dependent activity of soluble amyloid oligomers in protein misfolding diseases. *J. Biol. Chem.* **279,** 46363–46366
9. Lin, H., Zhu, Y. J., and Lal, R. (1999) Amyloid β protein (1–40) forms calcium-permeable, Zn^{2+}-sensitive channel in reconstituted lipid vesicles. *Biochemistry* **38,** 11189–11196
10. Pollard, H. B., Arispe, N., and Rojas, E. (1995) Ion channel hypothesis for Alzheimer amyloid peptide neurotoxicity. *Cell. Mol. Neurobiol.* **15,** 513–526
11. Walsh, D. M., and Selkoe, D. J. (2007) A β oligomers–A decade of discovery. *J. Neurochem.* **101,** 1172–1184
12. Quist, A., Doudevski, I., Lin, H., Azimova, R., Ng, D., Frangione, B., Kagan, B., Ghiso, J., and Lal, R. (2005) Amyloid ion channels: A common structural link for protein misfolding disease. *Proc. Natl. Acad. Sci. U.S.A.* **102,** 10427–10432
13. Bemporad, F., and Chiti, F. (2012) Protein misfolded oligomers: experimental approaches, mechanism of formation, and structure-toxicity relationships. *Chem. Biol.* **19,** 315–327
14. Fändrich, M. (2012) Oligomeric intermediates in amyloid formation: Structure determination and mechanisms of toxicity. *J. Mol. Biol.* **421,** 427–440
15. Kayed, R., Pensalfini, A., Margol, L., Sokolov, Y., Sarsoza, F., Head, E., Hall, J., and Glabe, C. (2009) Annular protofibrils are a structurally and functionally distinct type of amyloid oligomer. *J. Biol. Chem.* **284,** 4230–4237
16. Brender, J. R., Salamekh, S., and Ramamoorthy, A. (2012) Membrane disruption and early events in the aggregation of the diabetes related peptide IAPP from a molecular perspective. *Acc. Chem. Res.* **45,** 454–462
17. Shai, Y. (1999) Mechanism of the binding, insertion, and destabilization of phospholipid bilayer membranes by α-helical antimicrobial and cell nonselective membrane-lytic peptides. *Biochim. Biophys. Acta* **1462,** 55–70
18. Yeaman, M. R., and Yount, N. Y. (2003) Mechanisms of antimicrobial peptide action and resistance. *Pharmacol. Rev.* **55,** 27–55
19. Yip, C. M., Darabie, A. A., and McLaurin, J. (2002) Aβ42-peptide assembly on lipid bilayers. *J. Mol. Biol.* **318,** 97–107
20. Yip, C. M., Elton, E. A., Darabie, A. A., Morrison, M. R., and McLaurin, J. (2001) Cholesterol, a modulator of membrane-associated Aβ-fibrillogenesis and neurotoxicity. *J. Mol. Biol.* **311,** 723–734
21. Williamson, R., and Sutherland, C. (2011) Neuronal membranes are key to the pathogenesis of Alzheimers disease: the role of both raft and non-raft membrane domains. *Curr. Alzheimer Res.* **8,** 213–221
22. Castro, B. M., de Almeida, R. F., Goormaghtigh, E., Fedorov, A., and Prieto, M. (2011) Organization and dynamics of Fas transmembrane domain in raft membranes and modulation by ceramide. *Biophys. J.* **101,** 1632–1641
23. Gajate, C., Gonzalez-Camacho, F., and Mollinedo, F. (2009) Lipid raft connection between extrinsic and intrinsic apoptotic pathways. *Biochem. Biophys. Res. Commun.* **380,** 780–784
24. Forloni, G., Angeretti, N., Chiesa, R., Monzani, E., Salmona, M., Bugiani, O., and Tagliavini, F. (1993) Neurotoxicity of a prion protein fragment. *Nature* **362,** 543–546
25. Salmona, M., Malesani, P., De Gioia, L., Gorla, S., Bruschi, M., Molinari, A., Della Vedova, F., Pedrotti, B., Marrari, M. A., Awan, T., Bugiani, O., Forloni, G., and Tagliavini, F. (1999) Molecular determinants of the physicochemical properties of a critical prion protein region comprising residues 106–126. *Biochem. J.* **342,** 207–214
26. Selvaggini, C., De Gioia, L., Cantù, L., Ghibaudi, E., Diomede, L., Passerini, F., Forloni, G., Bugiani, O., Tagliavini, F., and Salmona, M. (1993) Molecular characteristics of a protease-resistant, amyloidogenic and neurotoxic peptide homologous to residues 106–126 of the prion protein. *Biochem. Biophys. Res. Commun.* **194,** 1380–1386
27. Brown, D. R. (1998) Prion protein-overexpressing cells show altered response to a neurotoxic prion protein peptide. *J. Neurosci. Res.* **54,** 331–340
28. Deli, M. A., Sakaguchi, S., Nakaoke, R., Abrahám, C. S., Takahata, H., Kopacek, J., Shigematsu, K., Katamine, S., and Niwa, M. (2000) PrP fragment 106–126 is toxic to cerebral endothelial cells expressing PrP(C). *Neuroreport* **11,** 3931–3936
29. Fioriti, L., Quaglio, E., Massignan, T., Colombo, L., Stewart, R. S., Salmona, M., Harris, D. A., Forloni, G., and Chiesa, R. (2005) The neurotoxicity of prion protein (PrP) peptide 106–126 is independent of the expression level of PrP and is not mediated by abnormal PrP species. *Mol. Cell. Neurosci.* **28,** 165–176
30. Kurganov, B., Doh, M., and Arispe, N. (2004) Aggregation of liposomes induced by the toxic peptides Alzheimer's Aβs, human amylin and prion(106–126): facilitation by membrane-bound G_{M1} ganglioside. *Peptides* **25,** 217–232
31. Thellung, S., Florio, T., Villa, V., Corsaro, A., Arena, S., Amico, C., Robello, M., Salmona, M., Forloni, G., Bugiani, O., Tagliavini, F., and Schettini, G. (2000) Apoptotic cell death and impairment of L-type voltage-sensitive calcium channel activity in rat cerebellar granule cells treated with the prion protein fragment 106–126. *Neurobiol. Dis.* **7,** 299–309
32. Salmona, M., Forloni, G., Diomede, L., Algeri, M., De Gioia, L., Angeretti, N., Giaccone, G., Tagliavini, F., and Bugiani, O. (1997) A neurotoxic and gliotrophic fragment of the prion protein increases plasma membrane microviscosity. *Neurobiol. Dis.* **4,** 47–57
33. Carimalo, J., Cronier, S., Petit, G., Peyrin, J. M., Boukhtouche, F., Arbez, N., Lemaigre-Dubreuil, Y., Brugg, B., and Miquel, M. C. (2005) Activation of the JNK-c-Jun pathway during the early phase of neuronal apoptosis induced by PrP106–126 and prion infection. *Eur. J. Neurosci.* **21,** 2311–2319
34. Kourie, J. I., Farrelly, P. V., and Henry, C. L. (2001) Channel activity of deamidated isoforms of prion protein fragment 106–126 in planar lipid bilayers. *J. Neurosci. Res.* **66,** 214–220
35. Lin, M. C., Mirzabekov, T., and Kagan, B. (1997) Channel formation by a neurotoxic prion protein fragment. *J. Biol. Chem.* **272,** 44–47
36. Ettaiche, M., Pichot, R., Vincent, J. P., and Chabry, J. (2000) *In vivo* cytotoxicity of the prion protein fragment 106–126. *J. Biol. Chem.* **275,** 36487–36490
37. Walsh, P., Neudecker, P., and Sharpe, S. (2010) Structural properties and dynamic behaviour of non-fibrillar oligomers formed by PrP(106–126). *J. Am. Chem. Soc.* **132,** 7684–7695
38. Walsh, P., Simonetti, K., and Sharpe, S. (2009) Core structure of amyloid fibrils formed by residues 106–126 of the human prion protein. *Structure* **17,** 417–426
39. Walsh, P., Yau, J., Simonetti, K., and Sharpe, S. (2009) Morphology and secondary structure of stable β-oligomers formed by the amyloid peptide PrP(106–126). *Biochemistry* **48,** 5779–5781
40. Oreopoulos, J., and Yip, C. M. (2009) Probing membrane order and topography in supported lipid bilayers by combined polarized total internal reflection fluorescence atomic force microscopy. *Biophys. J.* **96,** 1970–1984
41. Falsig, J., and Aguzzi, A. (2008) The prion organotypic slice culture assay–POSCA. *Nat. Protoc.* **3,** 555–562
42. Miret, S., De Groene, E. M., and Klaffke, W. (2006) Comparison of *in vitro* assays of cellular toxicity in the human hepatic cell line HepG2. *J. Biomol. Screen.* **11,** 184–193
43. Bertrand, R., Solary, E., O'Connor, P., Kohn, K. W., and Pommier, Y. (1994) Induction of a common pathway of apoptosis by staurosporine. *Exp. Cell Res.* **211,** 314–321
44. Moore, A., Donahue, C. J., Bauer, K. D., and Mather, J. P. (1998) Simultaneous measurement of cell cycle and apoptotic cell death. *Methods Cell Biol.* **57,** 265–278
45. Mor, A., Nguyen, V. H., Delfour, A., Migliore-Samour, D., and Nicolas, P. (1991) Isolation, amino acid sequence, and synthesis of dermaseptin, a novel antimicrobial peptide of amphibian skin. *Biochemistry* **30,** 8824–8830
46. Domingues, T. M., Riske, K. A., and Miranda, A. (2010) Revealing the lytic

mechanism of the antimicrobial peptide gomesin by observing giant unilamellar vesicles. *Langmuir* **26,** 11077–11084
47. Russell, A. L., Kennedy, A. M., Spuches, A. M., Venugopal, D., Bhonsle, J. B., and Hicks, R. P. (2010) Spectroscopic and thermodynamic evidence for antimicrobial peptide membrane selectivity. *Chem. Phys. Lipids* **163,** 488–497
48. Kendall, D. A., and MacDonald, R. C. (1982) A fluorescence assay to monitor vesicle fusion and lysis. *J. Biol. Chem.* **257,** 13892–13895
49. Yip, C. M., and McLaurin, J. (2001) Amyloid-β peptide assembly: a critical step in fibrillogenesis and membrane disruption. *Biophys. J.* **80,** 1359–1371
50. Nagle, J. F., and Tristram-Nagle, S. (2000) Structure of lipid bilayers. *Biochim. Biophys. Acta* **1469,** 159–195
51. Kučerka, N., Nieh, M.-P., and Katsaras, J. (2011) Fluid phase lipid areas and bilayer thicknesses of commonly used phosphatidylcholines as a function of temperature. *Biochim. Biophys. Acta* **1808,** 2761–2771
52. Seelig, J. (1978) 31P nuclear magnetic resonance and the head group structure of phospholipids in membranes. *Biochim. Biophys. Acta* **515,** 105–140
53. Ramamoorthy, A., Thennarasu, S., Lee, D. K., Tan, A., and Maloy, L. (2006) Solid-state NMR investigation of the membrane-disrupting mechanism of antimicrobial peptides MSI-78 and MSI-594 derived from magainin 2 and melittin. *Biophys. J.* **91,** 206–216
54. Baumgart, T., Hunt, G., Farkas, E. R., Webb, W. W., and Feigenson, G. W. (2007) Fluorescence probe partitioning between Lo/Ld phases in lipid membranes. *Biochim. Biophys. Acta* **1768,** 2182–2194
55. Feigenson, G. W. (2006) Phase behavior of lipid mixtures. *Nat. Chem. Biol.* **2,** 560–563
56. Hicks, D. A., Nalivaeva, N. N., and Turner, A. J. (2012) Lipid rafts and Alzheimer's disease: protein-lipid interactions and perturbation of signaling. *Front. Physiol.* **3,** 189
57. Malchiodi-Albedi, F., Paradisi, S., Matteucci, A., Frank, C., and Diociaiuti, M. (2011) Amyloid oligomer neurotoxicity, calcium dysregulation, and lipid rafts. *Int. J. Alzheimers Dis.* 10.4061/2011/906964
58. Wood, W. G., Schroeder, F., Igbavboa, U., Avdulov, N. A., and Chochina, S. V. (2002) Brain membrane cholesterol domains, aging and amyloid peptides. *Neurobiol. Aging* **23,** 685–694
59. Korlach, J., Schwille, P., Webb, W. W., and Feigenson, G. W. (1999) Characterization of lipid bilayer phases by confocal microscopy and fluorescence correlation spectroscopy. *Proc. Natl. Acad. Sci. U.S.A.* **96,** 8461–8466
60. Axelrod, D. (1989) in *Fluorescence Polarization Microscopy* (Langsing, T., and Wang, Y., eds) Vol. 30, pp. 333–352, Academic Press, San Diego
61. Timbs, M. M., and Thompson, N. L. (1990) Slow rotational mobilities of antibodies and lipids associated with substrate-supported phospholipid monolayers as measured by polarized fluorescence photobleaching recovery. *Biophys. J.* **58,** 413–428
62. Spink, C. H., Yeager, M. D., and Feigenson, G. W. (1990) Partitioning behavior of indocarbocyanine probes between coexisting gel and fluid phases in model membranes. *Biochim. Biophys. Acta* **1023,** 25–33
63. Oreopoulos, J., and Yip, C. M. (2009) Combinatorial microscopy for the study of protein-membrane interactions in supported lipid bilayers: Order parameter measurements by combined polarized TIRFM/AFM. *J. Struct. Biol.* **168,** 21–36
64. Taylor, M. G., Akiyama, T., Saitô, H., and Smith, I. C. (1982) Direct observation of the properties of cholesterol in membranes by deuterium NMR. *Chem. Phys. Lipids.* **31,** 359–379
65. Glabe, C. G. (2006) Common mechanisms of amyloid oligomer pathogenesis in degenerative disease. *Neurobiol. Aging* **27,** 570–575
66. Florio, T., Thellung, S., Amico, C., Robello, M., Salmona, M., Bugiani, O., Tagliavini, F., Forloni, G., and Schettini, G. (1998) Prion protein fragment 106–126 induces apoptotic cell death and impairment of L-type voltage-sensitive calcium channel activity in the GH3 cell line. *J. Neurosci. Res.* **54,** 341–352
67. Silei, V., Fabrizi, C., Venturini, G., Salmona, M., Bugiani, O., Tagliavini, F., and Lauro, G. M. (1999) Activation of microglial cells by PrP and β-amyloid fragments raises intracellular calcium through L-type voltage sensitive calcium channels. *Brain Res.* **818,** 168–170
68. Zhong, J., Zheng, W., Huang, L., Hong, Y., Wang, L., Qiu, Y., and Sha, Y. (2007) PrP106–126 amide causes the semi-penetrated poration in the supported lipid bilayers. *Biochim. Biophys. Acta* **1768,** 1420–1429
69. Brown, D. R., Schmidt, B., and Kretzschmar, H. A. (1996) Role of microglia and host prion protein in neurotoxicity of a prion protein fragment. *Nature* **380,** 345–347
70. Gu, Y., Fujioka, H., Mishra, R. S., Li, R., and Singh, N. (2002) Prion peptide 106–126 modulates the aggregation of cellular prion protein and induces the synthesis of potentially neurotoxic transmembrane PrP. *J. Biol. Chem.* **277,** 2275–2286
71. Pietri, M., Caprini, A., Mouillet-Richard, S., Pradines, E., Ermonval, M., Grassi, J., Kellermann, O., and Schneider, B. (2006) Overstimulation of PrPC signaling pathways by prion peptide 106–126 causes oxidative injury of bioaminergic neuronal cells. *J. Biol. Chem.* **281,** 28470–28479
72. Brender, J. R., Dürr, U. H., Heyl, D., Budarapu, M. B., and Ramamoorthy, A. (2007) Membrane fragmentation by an amyloidogenic fragment of human islet amyloid polypeptide detected by solid-state NMR spectroscopy of membrane nanotubes. *Biochim. Biophys. Acta* **1768,** 2026–2029
73. Kagan, B. L., Jang, H., Capone, R., Teran Arce, F., Ramachandran, S., Lal, R., and Nussinov, R. (2012) Antimicrobial activities of amyloid peptides. *Mol. Pharm.* **9,** 708–717
74. McMullen, T. P., Lewis, R. N., and McElhaney, R. N. (2004) Cholesterol-phospholipid interactions, the liquid-ordered phase and lipid rafts in model and biological membranes. *Curr. Opin. Colloid Interface Sci.* **8,** 459–468
75. Owen, D. M., Williamson, D. J., Magenau, A., and Gaus, K. (2012) Sub-resolution lipid domains exist in the plasma membrane and regulate protein diffusion and distribution. *Nat. Commun.* **3,** 1256
76. Kaiser, H.-J., Lingwood, D., Levental, I., Sampaio, J. L., Kalvodova, L., Rajendran, L., and Simons, K. (2009) Order of lipid phases in model and plasma membranes. *Proc. Natl. Acad. Sci. U.S.A.* **106,** 16645–16650
77. George, K. S., and Wu, S. (2012) Lipid raft: A floating island of death or survival. *Toxicol. Appl. Pharmacol.* **259,** 311–319
78. Cecchi, C., Nichino, D., Zampagni, M., Bernacchioni, C., Evangelisti, E., Pensalfini, A., Liguri, G., Gliozzi, A., Stefani, M., and Relini, A. (2009) A protective role for lipid raft cholesterol against amyloid-induced membrane damage in human neuroblastoma cells. *Biochim. Biophys. Acta* **1788,** 2204–2216
79. Bucciantini, M., Nosi, D., Forzan, M., Russo, E., Calamai, M., Pieri, L., Formigli, L., Quercioli, F., Soria, S., Pavone, F., Savistchenko, J., Melki, R., and Stefani, M. (2012) Toxic effects of amyloid fibrils on cell membranes: the importance of ganglioside GM1. *FASEB J.* **26,** 818–831
80. Comellas, G., Lemkau, L. R., Zhou, D. H., George, J. M., and Rienstra, C. M. (2012) Structural intermediates during α-synuclein fibrillogenesis on phospholipid vesicles. *J. Am. Chem. Soc.* **134,** 5090–5099
81. Lu, J. X., Yau, W. M., and Tycko, R. (2011) Evidence from solid-state NMR for nonhelical conformations in the transmembrane domain of the amyloid precursor protein. *Biophys. J.* **100,** 711–719
82. Smith, P. E., Brender, J. R., and Ramamoorthy, A. (2009) Induction of negative curvature as a mechanism of cell toxicity by amyloidogenic peptides: the case of islet amyloid polypeptide. *J. Am. Chem. Soc.* **131,** 4470–4478